

Interplay between Ferroelectricity and Metallicity in BaTiO₃

Veronica F. Michel, Tobias Esswein,* and Nicola A. Spaldin

Materials Theory, Department of Materials, ETH Zürich, Wolfgang-Pauli-Strasse 27, 8093 Zürich, Switzerland

*Corresponding author: *tobias.esswein@mat.ethz.ch*

Electronic Supplementary Information

If not otherwise specified in the caption of the figures, the computational parameters used correspond to the ones described in the methods section of the main text.

1 Undoped Tetragonal BaTiO₃

Berry-phase Calculation

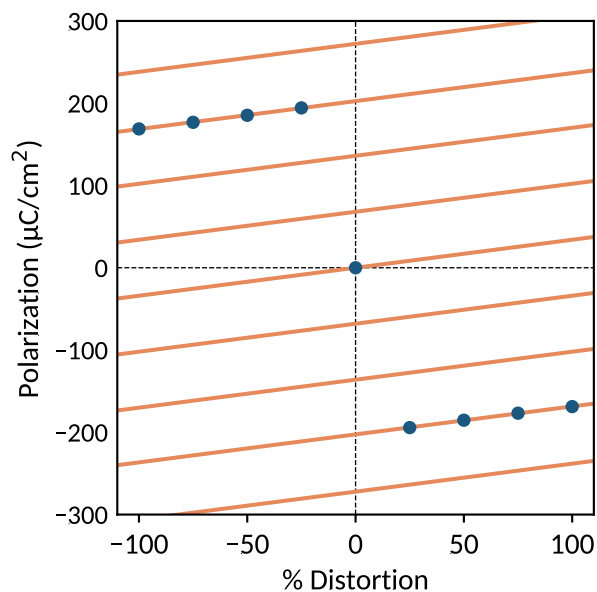


Figure 1: Berry-phase calculation for tetragonal BaTiO₃. The calculated spontaneous polarization of the system is 34 μC/cm².

2 Background-charge Doped Pseudocubic BaTiO₃ Unit Cell

Density of States

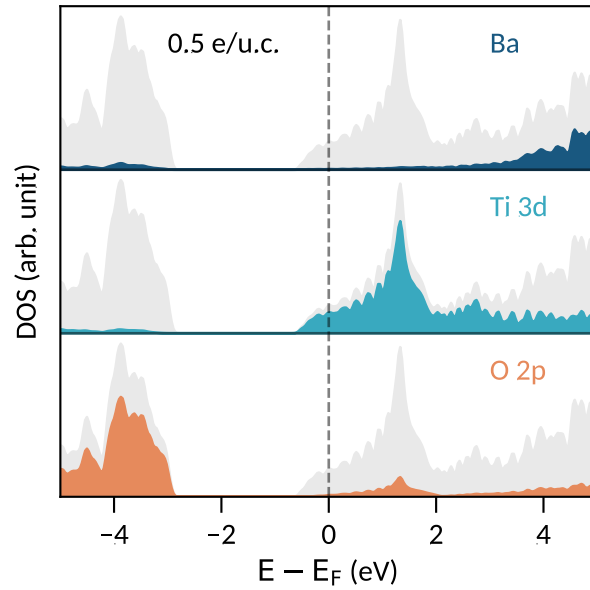


Figure 2: Density of states for pseudocubic BaTiO₃ doped with 0.5 e/u.c.

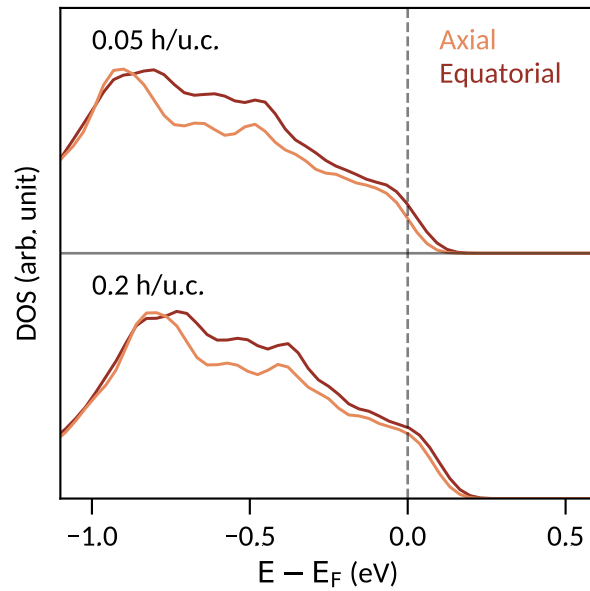


Figure 3: Oxygen site-resolved densities of states for pseudocubic BaTiO₃ doped with 0.05 h/u.c. (top) and 0.2 h/u.c. (bottom).

3 Impurity-doped BaTiO₃ Supercells

Polarization, Volume and Tetragonality

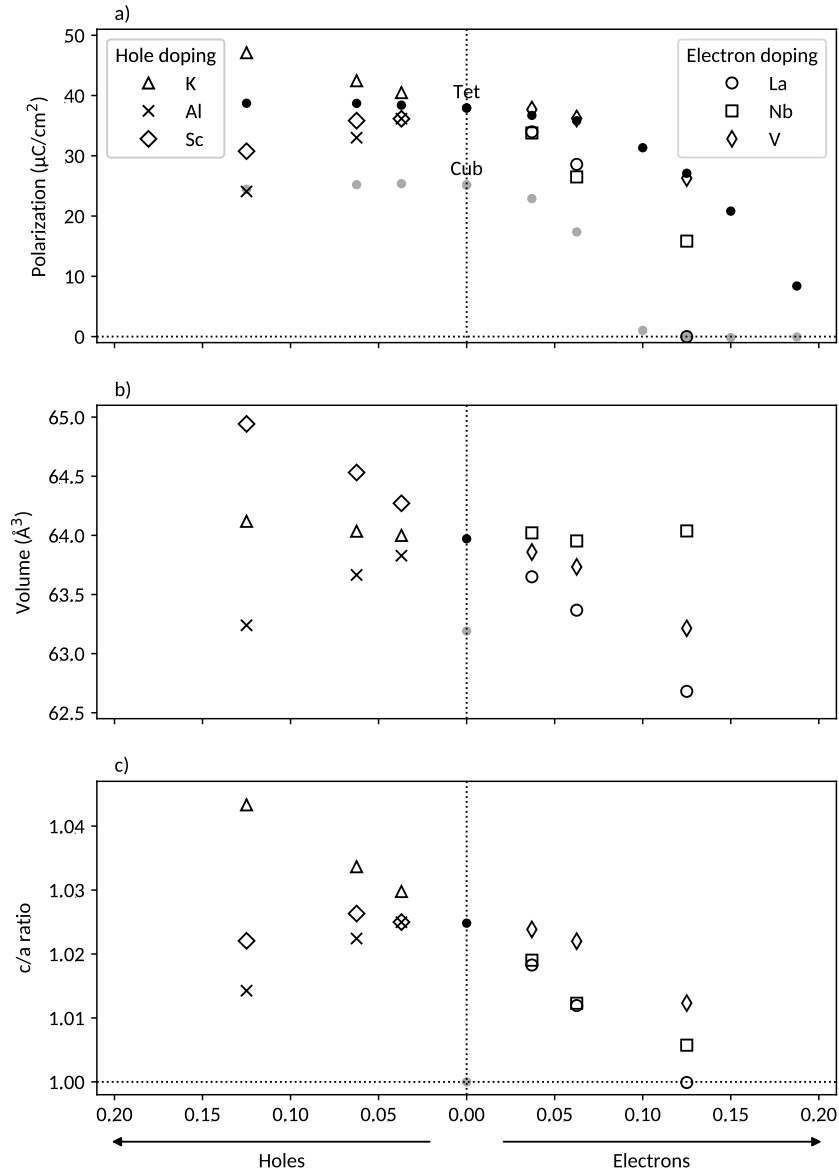


Figure 4: Polarization (a), average volume (b) and c/a ratio (c) of doped BaTiO₃ as a function of the charge-carrier concentration (electrons on the right, holes on the left). The charge carriers are introduced through doping with impurity atoms in $2 \times 2 \times 2$, $2\sqrt{2} \times 2\sqrt{2} \times 2$ and $3 \times 3 \times 3$ supercells and their charge-carrier concentrations are 0.125, and 0.0625 and 0.037 carriers/u.c., respectively. The k-point grids used for these calculations are $12 \times 12 \times 12$, $6 \times 6 \times 6$ and $4 \times 4 \times 4$, respectively. The systems are labeled with the name of their respective dopant. The black and grey dots correspond to the tetragonal and pseudocubic background-charge references.

Bond Ratios

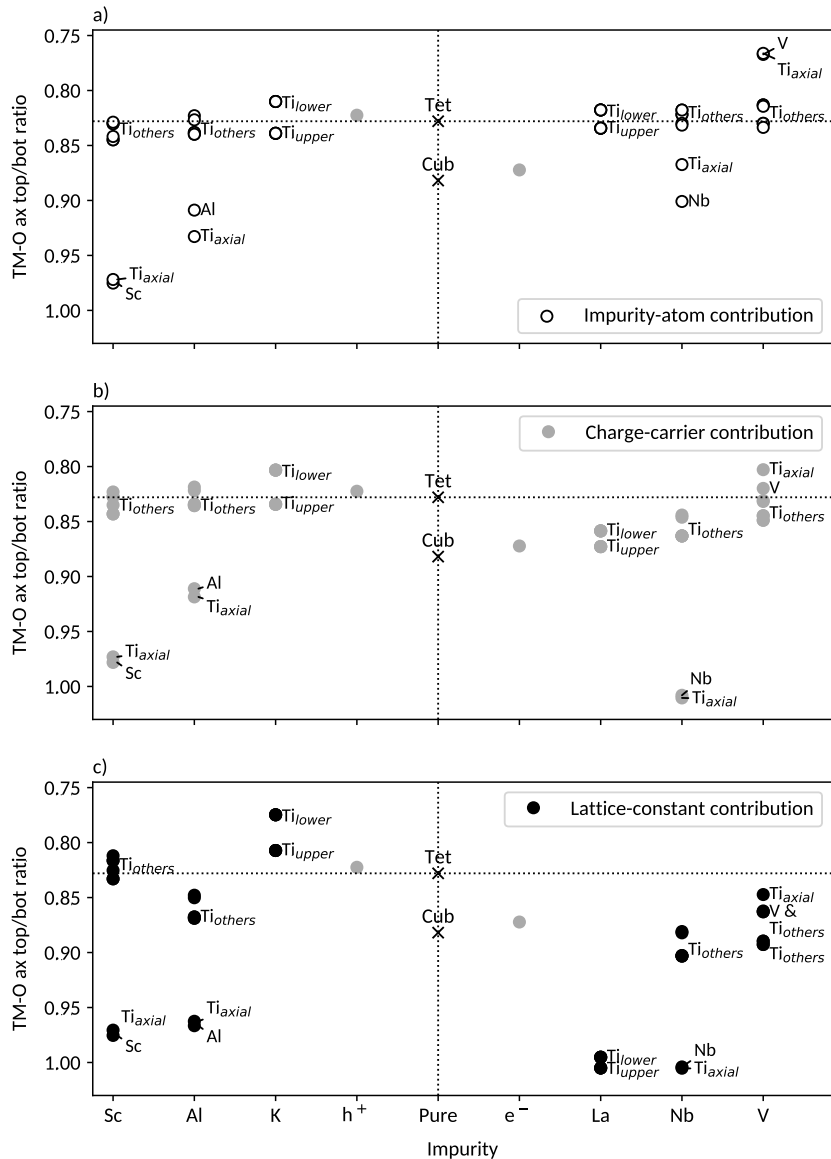


Figure 5: Bond ratios of the transition metal - oxygen axial top to bottom bonds for tetragonal BaTiO₃. a) Impurity-atom contribution with the impurity atom, 0 carriers/u.c. and fixed lattice constants (white circles), b) Charge-carrier contribution with the impurity atom, 0.125 carriers/u.c. and fixed lattice constants (grey circles) and c) Lattice-constant contribution with the impurity atom, 0.125 carriers/u.c. and free lattice constants (black circles). The impurity atom is indicated on the x-axis. Each system corresponds to a 2×2×2 supercell and therefore has eight bond ratio values (for its eight transition metals), partly overlapping. Pure BaTiO₃ in tetragonal and pseudocubic symmetry (abbreviated *tet* and *cub*) as well as background-charge doped tetragonal systems (holes: h⁺, electrons: e⁻) are given as a reference.

Density of States

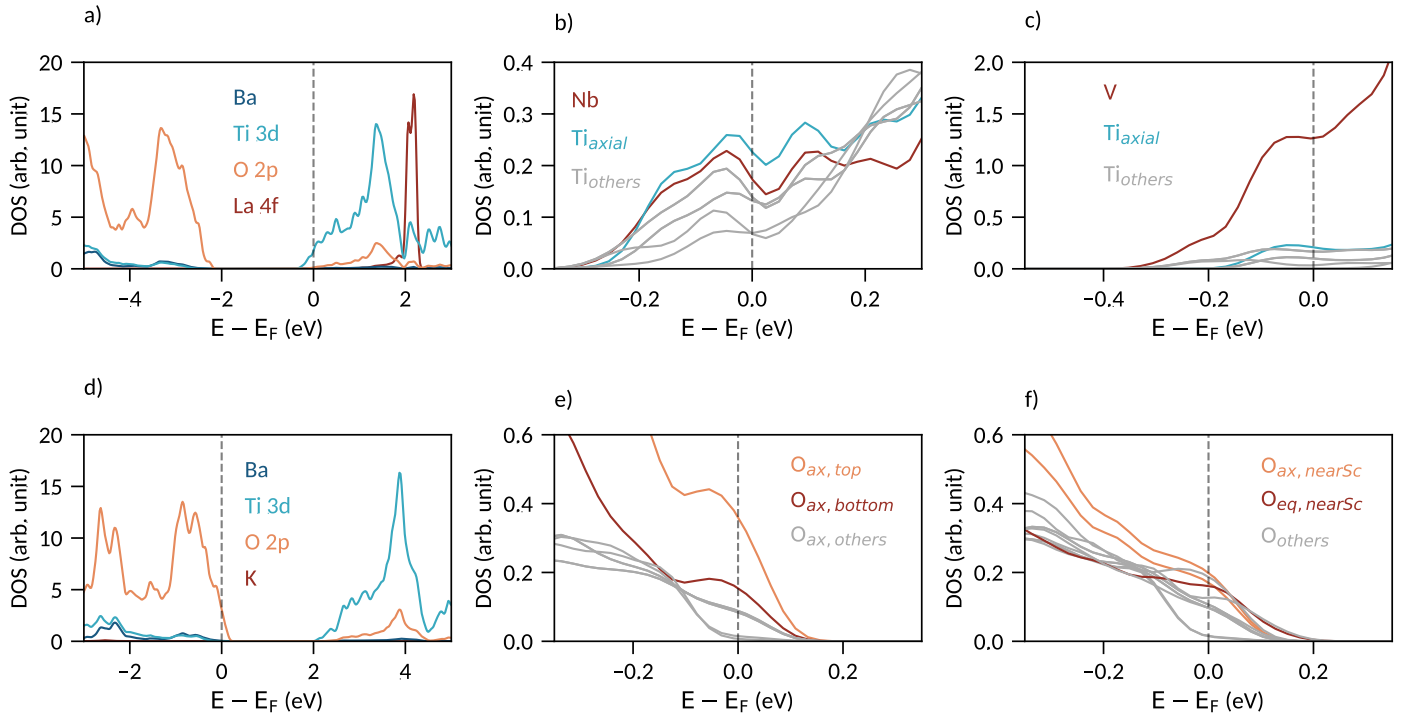


Figure 6: a) Density of states for La-doped BaTiO_3 (with one La in a $2 \times 2 \times 2$ BaTiO_3 supercell with fixed lattice constants). As the La introduces one valence electron into the system, the Fermi energy lies in the conduction band. The La f-states lie at higher energies and the main contribution to the conduction band comes from the Ti d orbitals. b) Transition-metal site-resolved density of states of Nb-doped BaTiO_3 (BTNO with one Nb in a $2 \times 2 \times 2$ BaTiO_3 supercell and fixed lattice constants). The region around the Fermi energy in the conduction band is shown. Two sites, the Nb and its axial neighboring Ti along the polar axis, have particularly large contributions. c) Transition-metal site-resolved density of states for V-doped BaTiO_3 (with one V in a $2 \times 2 \times 2$ BaTiO_3 supercell with fixed lattice constants). The conduction band region around the Fermi energy is shown. The V has a particularly large contribution, whereas the its axial neighboring Ti along the polar axis hardly contributes to the conduction band. d) Density of states for K-doped BaTiO_3 (BKTO with one K in a $2 \times 2 \times 2$ BaTiO_3 supercell and fixed lattice constants). One valence electron is depleted from the system so that the Fermi energy lies in the valence band. The K does not affect the DOS around the Fermi energy. e) Axial oxygen site-resolved density of states of Al-doped BaTiO_3 (with one Al in a $2 \times 2 \times 2$ BaTiO_3 supercell with fixed lattice constants). The most contributing sites are the axial oxygens around the Al atom (top and bottom). f) Oxygen site-resolved density of states of Sc-doped BaTiO_3 (BTSO with one Sc in a $2 \times 2 \times 2$ BaTiO_3 supercell and fixed lattice constants). The most contributing sites are the axial and equatorial oxygens around the Sc atom. All the supercells have tetragonal symmetry. All DOS are computed with a $12 \times 12 \times 12$ k-point grid.